Available online at www.sciencedirect.com
ScienceDirect
International Journal of Thermal Sciences 47 (2008) 1148–1157
International Journal of Thermal Sciences
www.elsevier.com/locate/ijts

On the experimental determination of flame front positions and of propagation parameters for a fire

K. Chetehouna [a,*], O. Séro-Guillaume [b], I. Sochet [a], A. Degiovanni [b]

[a] *Laboratoire Energétique Explosions Structures, ENSI de Bourges, 88 boulevard Lahitolle, 18020 Bourges Cedex, France*
[b] *Laboratoire d'Energétique et de Mécanique Théorique et Appliquée CNRS–UMR 7563, ENSEM–INPL, 02 avenue de la forêt de Haye, B.P. 160, 54504 Vandoeuvre cedex, France*

Received 5 December 2006; received in revised form 7 October 2007; accepted 11 October 2007

Available online 26 November 2007

Abstract

This work proposes a new method for determining the fire front positions for optically thin flames and the rate of spread (*ROS*) of forest or vegetation fires. It is based on an application for linear flame fronts that are generated in a fire tunnel with known dimensions using Quercus coccifera shrubs as vegetal fuel. In the first step of the method, the heat fluxes coming from the flame are measured by a specific thermal sensor in four horizontal directions. In the second, these heat fluxes are calculated theoretically using an approximate resolution of the radiative transfer equation. Subsequently, the positions of the fire front and the flame characteristics are determined by applying an inverse method. The rate of spread is deduced by applying a least-square regression on the position values. An extrapolation of this new method to more complex experimental scenarios such as prescribed burnings is proposed.

Keywords: Heat flux sensor; Fire experiments; Flame model; Fire front positions; Rate of spread; Characteristics of flame

1. Introduction

Over the last decade, immense forested areas of the planet have one by one blazed up. In 1997, the forests of Malaysia and Indonesia were the first to be devastated by massive fires; next, in 1998, the Brazilian Amazon, the Palawan Island in Philippines were in turn burned, and later the same year it was Mexico. In 2003, 2004 and 2005, hundreds of thousands of hectares of forests of Mediterranean countries, such as Morocco, Algeria, Portugal, Spain, Italy, Greece and France, were in flames throughout the summer. Simulation of forest fire propagation can serve several purposes. The prevision of the fire front position can help firemen to optimise the distribution of fighting means, which supposes real time simulation. Another application of simulation relates to fire prevention. Using terrain data, computer models of propagation could provide information on dangerous areas. The possibility for such models to take into account some aspects of means of fire fighting, such as chemical retardants, is highly desirable. However, currently the fire spreading simulators are far from being scientifically satisfactory. The main information provided by propagation models is the fire line position and any measurement system intended to validate the models should, at least, provide this position not only for laboratory experiments but also for real field experiments. Using heat flux measurements a first attempt at doing such identification for prescribed burning is reported in this paper.

It is generally admitted that the leading driving physical process involved in the propagation of forest fire is radiative transfer, cf. [1,2]. Therefore it seems relevant for such propagation to measure the radiative heat flux. Moreover a typical size for such experiments is fifty meters long (size of the plot to be burnt) and it is difficult to design apparatus giving thermal information on this scale, for example. The main idea is to replace local measurements, such as one given by thermocouples, by global flux measurements. We have thus designed a thermal sensor which measures the heat flux, cf. [3]. The aim of this paper is to show how this apparatus can provide the position of

* Corresponding author. Tel.: +33 248 484 065; fax: +33 248 484 050.
E-mail address: khaled.chetehouna@ensi-bourges.fr (K. Chetehouna).

1290-0729/$ – see front matter
doi:10.1016/j.ijthermalsci.2007.10.006

Nomenclature

a	absorption coefficient
B	Stefan–Boltzmann constant
C_{co}	copper plate capacity
C_{st}	steel frame capacity
e_j	flame thicknesses
f	frequency
f_c	cut-off frequency
H	magnitude of the transfer function for the filter
h_f	flame height
i	radiative intensity
i_b	radiative intensity of Blackbody
$\mathbf{i}, \mathbf{j}, \mathbf{n_i}, \mathbf{s}$	unit vectors
K	extinction coefficient
K_{air}	air extinction coefficient
K_f	flame extinction coefficient
K_v	vegetation extinction coefficient
l_f	flame length
N	number of the fire front positions ($N = 10$)
$\hat{R}, R_{e_1}, R_{e_2}$	thermal resistances
ROS	rate of spread
S	objective function
S_f	flame surface
$\Delta t_{i,i+1}$	time separating two successive temperature peaks
T_f	temperature of flame
T_v	temperature of vegetation
W	half the width of the combustion vat
Y_j	flame front positions

Greek symbols

φ_i^{exp}	experimental heat flux received by copper plate n° i
θ_{co_i}	temperature of copper plate n° i
θ_{st}	steel frame temperature
Φ_a^{th}	theoretical heat flux received by the front face of the sensor
Φ_l^{th}	theoretical heat flux received by the lateral faces of the sensor
Φ_1^{exp}	experimental heat flux received by face n° 1 of the sensor
Φ_2^{exp}	experimental heat flux received by face n° 2 of the sensor
Φ_4^{exp}	experimental heat flux received by face n° 4 of the sensor
$\tilde{\Phi}$	phase function
ω_i, ω	solid angle
$\mathrm{d}\Omega$	elementary volume of flame
Ω_f	flame domain
α_f	flame tilt angle
η	vector of flame parameters
α_j, β_j	weighting coefficients
σ_S	scattering coefficient

the fire front and can be used to identify some parameters of a flame model. Identification has been done with experiments in a fire tunnel with real vegetation but for a line fire front, we postpone to a further work the study of the identification of fire front with any shape. However we will present the objective function to be minimised in this general case.

The second section is devoted to the description of a designed thermal sensor. We will present in this paper only the specifications of the sensor and its transfer function. A detailed description of this apparatus was presented in [4]. In the third section we will derive a flame model from the radiative transfer equation. In the fourth section the instrumentation of the fire tunnel will be described as well as the experiment concerned. In section five we will consider the flame model developed in the third section and using the inverse method we will identify some parameters involved in this model. Moreover the position and the rate of spread will be measured for a fire tunnel experiment. An extension of the methodology for identifying the front in real experiments of fire is proposed in this section.

2. Description of the thermal sensor and the experimental heat fluxes

As explained in the introduction, the aim of the heat flux sensor is to determine the fire front positions and the flame characteristics. In order to instrument real fires, this sensor should satisfy the following conditions:

- it must be simple and convenient for installation and use;
- it must be as cheap as possible;
- it should not be destroyed by the flames;
- its scale is adapted to the one used in physical models of propagation [5–8];
- it can allow an average evaluation of heat flux, temperature of gases and their velocity;
- all of the acquisition is sent to a computer by a wireless connection (radio communication).

The heat flux sensor is made of a steel frame (thickness = 2 mm, thermal conductivity = 46 $\mathrm{W\,m^{-1}\,K^{-1}}$), a thermal insulating sheet (thickness = 6 mm, thermal conductivity = 0.23 $\mathrm{W\,m^{-1}\,K^{-1}}$), glue sheets (thickness = 5 mm, thermal conductivity = 0.29 $\mathrm{W\,m^{-1}\,K^{-1}}$), 4 small copper plates (thickness = 1 mm, thermal conductivity = 389 $\mathrm{W\,m^{-1}\,K^{-1}}$) and 9 type K thermocouples (diameter = 0.5 mm). The different analogical signals measured by this sensor are digitalised in a digitalisation module and transmitted to the computer by a transmitter antenna, cf. Fig. 1.

The transfer function, as is detailed in appendix, giving the heat flux received by each copper plate φ_i^{exp} [W] ($i = \overline{1,4}$) as a function of the measured temperature of the plate θ_{co_i}, can be written by:

$$\varphi_i^{\mathrm{exp}}(t) = C_{\mathrm{co}} \frac{\mathrm{d}\theta_{\mathrm{co}_i}}{\mathrm{d}t} + \left(\frac{1}{\hat{R}} + \frac{1}{R_{e_1}}\right)\theta_{\mathrm{co}_i} - \frac{1}{\hat{R}}\theta_{\mathrm{st}} \tag{1}$$

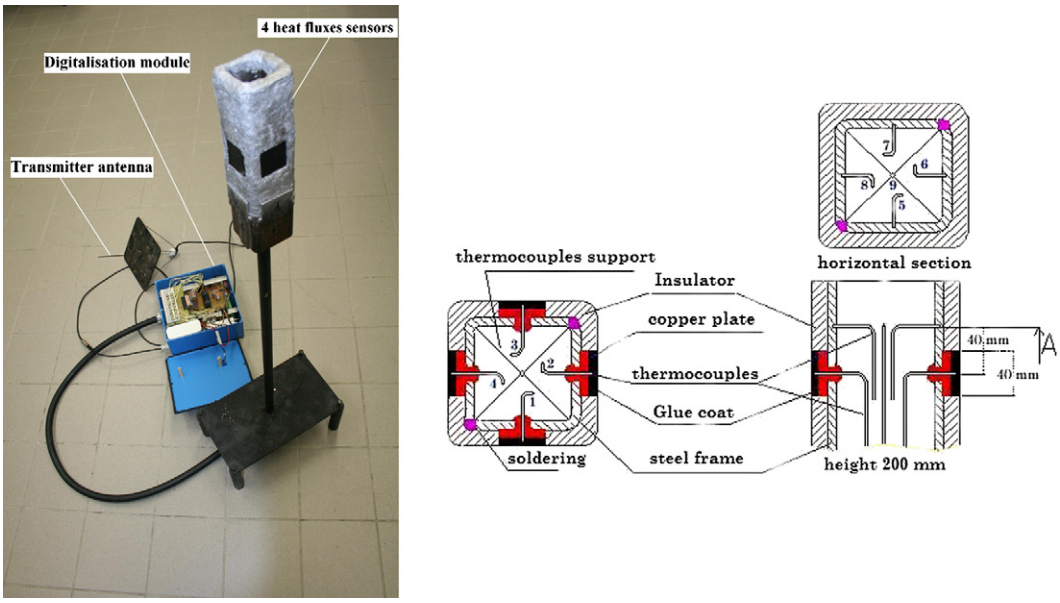

Fig. 1. Photograph of the heat flux sensor.

Table 1
Values of the parameters of the transfer function

R_{e_1} [K/W]	C_{co} [J/K]	$\hat{R}$ [K/W]
107.8	6.6	27.4

where C_{co} [J/K] is the capacity of the copper plate, $\hat{R}$ [K/W] is a thermal resistance modelling the contact between the copper plate and the steel frame, R_{e_1} [K/W] models the heat transfer between the sensor and the outside and θ_{st} [K] is the steel frame's temperature. The different parameters involved in the transfer function have been obtained by calibration experiments, cf. [3]. The values of these parameters are given in Table 1.

3. Mathematical modelling of the heat fluxes

The heat flux sensor, described above, is placed in the middle of the fire tunnel at a fixed point $\mathbf{M}(x_0, y_0)$ on top of the vegetation, cf. Fig. 2. We must calculate the theoretical heat fluxes emitted by the flame and received by the different faces of the sensor. In this model, the thermal effects of the lateral walls can be neglected.

The flame model considered in this paper is based on an approximate resolution of the radiative transfer equation, cf. [9], as explained below. In this mathematical modelling, the flame is assimilated to a parallelepiped with a variable thickness e_j, characterised by a height h_f, a tilt angle α_f, a temperature T_f, and an extinction coefficient K_f and supposed to move at the constant rate of spread R in each propagation zone. This rate of spread can be obtained by a least-squares regression based on the values of the flame front positions Y_j.

Let us consider some point $\mathbf{M}$ inside or just above the vegetation. A line $\mathbf{O_1M}$ crosses the flame in s_1, s_2 and the top of the vegetation in s_3, cf. Fig. 3. In this geometry, the radiative transfer equation can be written:

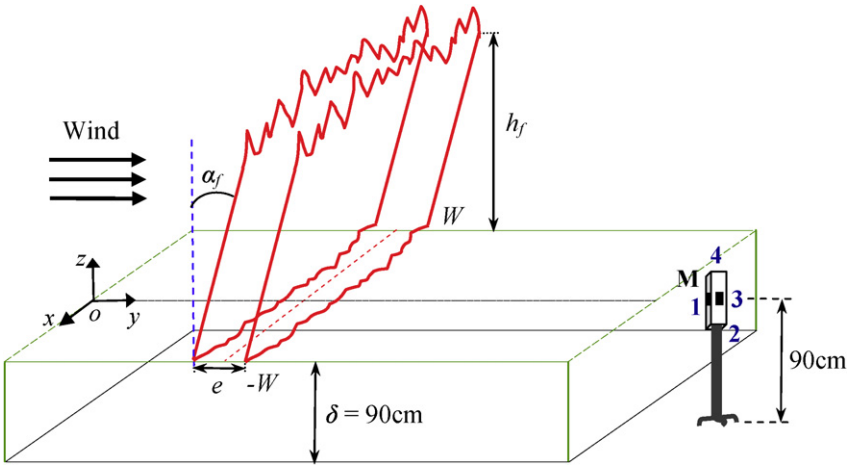

Fig. 2. Diagram of the vegetation-flame-sensor system.

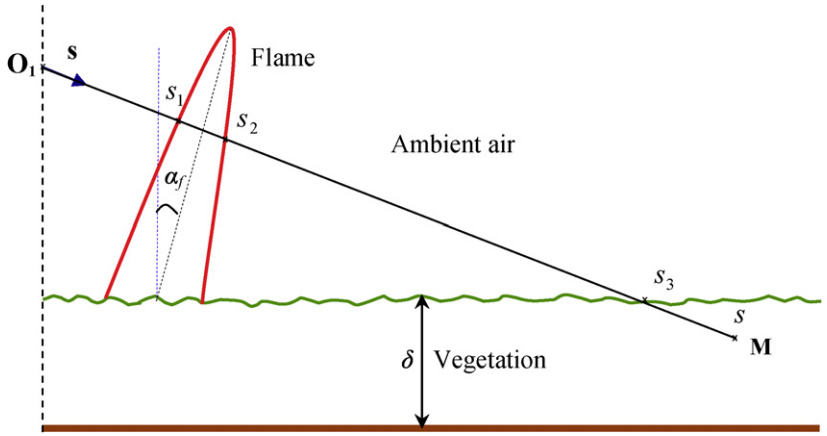

Fig. 3. Geometry for integration of the radiative transfer equation.

$$\frac{\mathrm{d}i}{\mathrm{d}s} = -K(s)i(s) + a(s)i_b(s) + \frac{\sigma_S(s)}{4\pi}\int_{\omega_i=0}^{4\pi} i(s,\omega_i)\tilde{\Phi}(\omega,\omega_i)\,\mathrm{d}\omega_i \quad (2)$$

where i is the radiative intensity, K, a and σ_S are respectively the extinction coefficient, the absorption coefficient and the scattering coefficient. $\tilde{\Phi}$ is the phase function and ω_i is the solid angle.

For ambient air, flame and vegetation the radiation coefficients K and a are supposed constant and the scattering coefficient σ_S is supposed to be null, cf. [6,10], so that the absorption coefficient becomes equal to the extinction coefficient. This hypothesis is not valid for optically intermediate flames. The extinction coefficient takes the following values:

(i) In $[0, s_1]$, $K = K_{\mathrm{air}} = 0$.
(ii) In $[s_1, s_2]$, $K = K_f$.
(iii) In $[s_2, s_3]$, $K = K_{\mathrm{air}} = 0$.
(iv) In $[s_3, s]$, $K = K_v$.

The radiative intensity at point **M** is then:

$$i(s) = K_f \mathrm{e}^{-K_v(s-s_3)}\int_{s_1}^{s_2} i_b(\bar{s})\mathrm{e}^{-K_f(s_2-\bar{s})}\,\mathrm{d}\bar{s} + K_v\int_{s_3}^{s} i_b(\bar{s})\mathrm{e}^{-K_v(s-\bar{s})}\,\mathrm{d}\bar{s} \quad (3)$$

with $i_b(\bar{s}) = i_b(T_f)$ in $[s_1, s_2]$ and $i_b(\bar{s}) = i_b(T_v)$ in $[s_3, s]$ where i_b is the radiative intensity of Blackbody. For sake of simplicity we can consider that the flame temperature is constant so that (3) can be written:

$$i(s) = \frac{BT_f^4}{\pi}\left(1-\mathrm{e}^{-K_f(s_2-s_1)}\right)\mathrm{e}^{-K_v(s-s_3)} + K_v\int_{s_3}^{s} i_b(\bar{s})\mathrm{e}^{-K_v(s-\bar{s})}\,\mathrm{d}\bar{s} \quad (4)$$

In a thin flame approximation $(1-\mathrm{e}^{-K_f(s_2-s_1)}) \approx K_f(s_2-s_1) = K_f\int_{s_1}^{s_2}\mathrm{d}\bar{s}$ and (4) becomes:

$$i(s) = K_f\frac{BT_f^4}{\pi}\mathrm{e}^{-K_v(s-s_3)}\int_{s_1}^{s_2}\mathrm{d}\bar{s} + K_v\int_{s_3}^{s} i_b(\bar{s})\mathrm{e}^{-K_v(s-\bar{s})}\,\mathrm{d}\bar{s} \quad (5)$$

The radiative heat flux received by face n° i of the thermal sensor with unit normal $\mathbf{n_i}$ is:

$$\varphi_i(\mathbf{M}) = \int_{\omega=0}^{4\pi} i(s)\mathbf{s}\cdot\mathbf{n_i}\,\mathrm{d}\omega \quad (6)$$

where $\mathrm{d}\omega$ is the elementary solid angle in the direction **s**. If we insert expression (5) in (6), we obtain:

$$\varphi_i(\mathbf{M}) = K_f\frac{B}{\pi}\int_{\omega=0}^{4\pi}\int_{s_1}^{s_2} T_f^4\mathrm{e}^{-K_v(s-s_3)}\mathbf{s}\cdot\mathbf{n_i}\,\mathrm{d}\bar{s}\,\mathrm{d}\omega + K_v\int_{\omega=0}^{4\pi}\int_{s_3}^{s} i_b(\bar{s})\mathrm{e}^{-K_v(s-\bar{s})}\mathbf{s}\cdot\mathbf{n_i}\,\mathrm{d}\bar{s}\,\mathrm{d}\omega \quad (7)$$

The last term of (7) is the contribution of the vegetation to the radiative heat flux. In order to characterise only the flame, this last term should be taken away. Let us notice that because we assume that the vegetal homogenised medium is isotropic, the contribution of the vegetation is the same in all directions and is given by the rear plate number 3. Thus the theoretical heat flux Φ_i^{th} received by the thermal sensor coming from the flame can be written:

$$\Phi_i^{\mathrm{th}}(\mathbf{M}) = \varphi_i(\mathbf{M}) - \varphi_3(\mathbf{M}) = K_f\frac{B}{\pi}\int_{\omega=0}^{4\pi}\int_{s_1}^{s_2} T_f^4\mathrm{e}^{-K_v(s-s_3)}\mathbf{s}\cdot\mathbf{n_i}\,\mathrm{d}\bar{s}\,\mathrm{d}\omega \quad (8)$$

If one replaces $\mathrm{d}\bar{s}\,\mathrm{d}\omega$ by $\frac{\mathrm{d}\Omega}{\mathbf{PM}^2}$ where $\mathrm{d}\Omega$ is an elementary volume of flame, the expression (8) becomes:

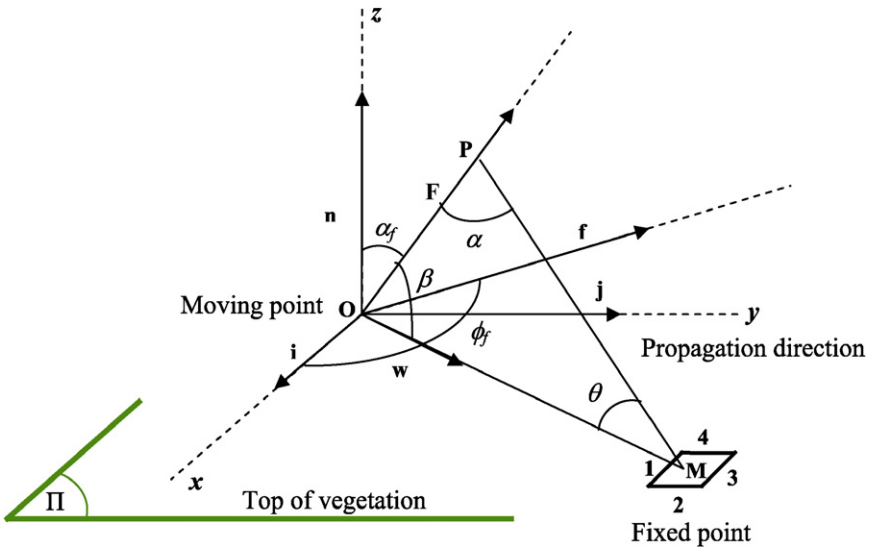

Fig. 4. Calculation geometry of the flame.

$$\Phi_i^{\text{th}}(\mathbf{M}) = K_f \frac{B}{\pi} \int\limits_{\Omega_f} T_f^4 \frac{\mathbf{s}\cdot\mathbf{n_i}}{\mathbf{PM}^2}\,\mathrm{d}\Omega \tag{9}$$

with Ω_f being the domain occupied by the flame.

We used the following denotations: $\mathbf{PM} = \rho$, $\mathbf{OP} = \xi\mathbf{F}$, $\alpha_f = (\mathbf{n}, \mathbf{F})$ where $\mathbf{F}$ is the unit vector directing the flame, cf. Fig. 4. The unit vector $\mathbf{f}$ is the projection of $\mathbf{F}$ on Π so that $\phi_f = (\mathbf{i}, \mathbf{f})$. $\mathbf{OM} = r\mathbf{w}$ where $\mathbf{w}$ is the unit vector of the line $\mathbf{OM}$, $\beta = (\mathbf{F}, \mathbf{w})$ and $\phi = (\mathbf{i}, \mathbf{w})$. In the triangle POM we define the angles $\alpha = \widehat{\mathrm{OPM}}$ and $\theta = \widehat{\mathrm{OMP}}$ so that $\alpha + \theta + \beta = \pi$. Let us note that:

$$\mathbf{F} = \sin\alpha_f \mathbf{f} + \cos\alpha_f \mathbf{n}$$
$$\mathbf{s} = \frac{\mathbf{PM}}{\rho} = \frac{\mathbf{OM} - \mathbf{OP}}{\rho} = \frac{r}{\rho}\mathbf{w} - \frac{\xi}{\rho}\mathbf{F} \tag{10}$$

Thus:

$$\mathbf{s}\cdot\mathbf{n_i} = \frac{r}{\rho}\mathbf{w}\cdot\mathbf{n_i} - \frac{\xi}{\rho}\mathbf{F}\cdot\mathbf{n_i} \tag{11}$$

Let us notice moreover that:

$$h_f = l_f \cos\alpha_f \tag{12}$$

where l_f is the length of the flame. This length is equal to the flame height h_f on experiments of fire without wind. So the theoretical heat flux Φ_i^{th} can be expressed as:

$$\Phi_i^{\text{th}}(\mathbf{M}) = K_f \frac{B}{\pi} \int\limits_{S_f} \frac{\mathrm{d}x\,\mathrm{d}y}{\cos\alpha_f} \int\limits_0^{l_f} \frac{T_f^4}{\rho^3}(r\mathbf{w}\cdot\mathbf{n_i} - \xi\mathbf{F}\cdot\mathbf{n_i})\,\mathrm{d}\xi \tag{13}$$

with S_f the area of flame on top of the vegetation. For the lateral faces of the heat flux sensor, we consider only half of this area.

In the present situation, the unit vector $\mathbf{n_i}$ has two values: $\mathbf{n_i} = \mathbf{i}$ (for the lateral faces) and $\mathbf{n_i} = \mathbf{j}$ (for the front face). Let us consider now these two configurations:

(1) Case where $\mathbf{n_i} = \mathbf{i}$.

We must calculate:

$$\Phi_l^{\text{th}}(\mathbf{M}) = K_f \frac{B}{\pi} \int\limits_{\frac{1}{2}S_f} \frac{\mathrm{d}x\,\mathrm{d}y}{\cos\alpha_f} \int\limits_0^{l_f} \frac{T_f^4}{\rho^3}(r\mathbf{w}\cdot\mathbf{i} - \xi\mathbf{F}\cdot\mathbf{i})\,\mathrm{d}\xi \tag{14}$$

If we insert $\mathbf{F} = \sin\alpha_f\mathbf{f} + \cos\alpha_f\mathbf{n}$ in this equation, we obtain:

$$\Phi_l^{\text{th}}(\mathbf{M}) = K_f \frac{B}{\pi} \int\limits_{\frac{1}{2}S_f} \frac{\mathrm{d}x\,\mathrm{d}y}{\cos\alpha_f} \times \int\limits_0^{l_f} \frac{T_f^4}{\rho^3}(r\cos\phi - \xi\sin\alpha_f\cos\phi_f)\,\mathrm{d}\xi \tag{15}$$

The sinus law in the triangle OPM provides the relation $\frac{\rho}{\sin\beta} = \frac{r}{\sin\alpha} = \frac{\xi}{\sin\theta}$ so that:

$$\rho = \frac{r\sin\beta}{\sin(\beta+\theta)}, \qquad \xi = \frac{r\sin\theta}{\sin(\beta+\theta)}$$
$$\mathrm{d}\xi = r\frac{\sin\beta}{\sin^2(\beta+\theta)}\,\mathrm{d}\theta \tag{16}$$

After some calculations, we can obtain this expression:

$$\Phi_l^{\text{th}}(\mathbf{M}) = K_f \frac{B}{\pi} \int\limits_{\frac{1}{2}S_f} T_f^4 \frac{\mathrm{d}x\,\mathrm{d}y}{r\sin^2\beta\cos\alpha_f} \times \left[(\cos\phi\cos\beta - \sin\alpha_f\cos\phi_f)(1-\cos\theta_f) + \cos\phi\sin\beta\sin\theta_f\right] \tag{17}$$

with $\cos\beta = \sin\alpha_f\cos(\phi - \phi_f)$, $\sin^2\beta = 1 - \sin^2\alpha_f\cos^2(\phi - \phi_f)$, $\cot\theta_f = \frac{r\cos\alpha_f}{h_f\sin\beta} - \cot\beta$.

(2) Case where $\mathbf{n_i} = \mathbf{j}$.

In this case we must calculate:

$$\Phi_a^{\text{th}}(\mathbf{M}) = K_f \frac{B}{\pi} \int\limits_{S_f} \frac{\mathrm{d}x\,\mathrm{d}y}{\cos\alpha_f} \int\limits_0^{l_f} \frac{T_f^4}{\rho^3}(r\mathbf{w}\cdot\mathbf{j} - \xi\mathbf{F}\cdot\mathbf{j})\,\mathrm{d}\xi \tag{18}$$

Let us notice moreover that $\mathbf{w}\cdot\mathbf{j}=\sin\phi$ and $\mathbf{F}\cdot\mathbf{j}=\sin\alpha_f\sin\phi_f$; the theoretical heat flux received by the front face of the thermal sensor can be written:

$$\Phi_a^{\text{th}}(\mathbf{M})=K_f\frac{B}{\pi}\int_{S_f}T_f^4\frac{\mathrm{d}x\,\mathrm{d}y}{r\sin^2\beta\cos\alpha_f}\times\left[(\sin\phi\cos\beta-\sin\alpha_f\sin\phi_f)(1-\cos\theta_f)+\sin\phi\sin\beta\sin\theta_f\right] \tag{19}$$

In this paper, we study only the case of propagation without wind $\alpha_f=0$. So, we have $\cos\alpha_f=1$, $\sin\alpha_f=\cos\beta=0$, $\sin\beta=1$ and $\theta_f=\operatorname{arctag}(\frac{h_f}{r})$. The heat fluxes $\Phi_a^{\text{th}}(\mathbf{M})$ and $\Phi_l^{\text{th}}(\mathbf{M})$ can be expressed now as:

$$\Phi_a^{\text{th}}(\mathbf{M})=K_f\frac{B}{\pi}\int_{S_f}T_f^4\frac{\sin\phi}{r}\sin\theta_f\,\mathrm{d}x\,\mathrm{d}y \tag{20}$$

$$\Phi_l^{\text{th}}(\mathbf{M})=K_f\frac{B}{\pi}\int_{\frac{1}{2}S_f}T_f^4\frac{\cos\phi}{r}\sin\theta_f\,\mathrm{d}x\,\mathrm{d}y \tag{21}$$

where $r=\sqrt{X^2+Y^2}$, $\sin\phi=\frac{Y}{r}$, $\cos\phi=\frac{X}{r}$ with $X=x_0-x$ and $Y=y_0-y$. If we use the new variables X and Y in these expressions, we obtain:

- *Face* 1 (*front face*):

$$\Phi_a^{\text{th}}(Y_j,e_j,h_f,T_f,K_f)=2K_f\frac{B}{\pi}\int_{Y_j+\frac{e_j}{2}}^{Y_j-\frac{e_j}{2}}\int_W^0 T_f^4\frac{Y}{X^2+Y^2}\sin\theta_f\,\mathrm{d}X\,\mathrm{d}Y \tag{22}$$

- *Faces* 2 *and* 4 (*lateral faces*):

$$\Phi_l^{\text{th}}(Y_j,e_j,h_f,T_f,K_f)=2K_f\frac{B}{\pi}\int_{Y_j+\frac{e_j}{2}}^{Y_j-\frac{e_j}{2}}\int_W^0 T_f^4\frac{X}{X^2+Y^2}\sin\theta_f\,\mathrm{d}X\,\mathrm{d}Y \tag{23}$$

4. Instrumentation and experiments in a fire tunnel

The measurement systems are composed of several apparatuses. The first one is an outside fire tunnel designed by the C.E.R.E.N. laboratory. This fire tunnel can experiment with a wind of 8 m/s velocity, and there is a linear ignition system, cf. Fig. 5.

The fuel used in this tunnel is Quercus coccifera, dominant vegetation in the Mediterranean region, where its average height is 90 cm. A straw layer 10 cm thick with a load (surface density) of 1.5 kg/m^2 was used as vegetable litter.

A heat flux sensor, a video camera and five thermocouples dedicated to the determination of the rate of spread have been used. The position of the different devices is indicated in Fig. 6.

Several fire experiments have been carried out in the fire tunnel in order to study the effect of the wind (6 experiments for a Quercus coccifera load of 3 kg/m^2 and wind values of 0, 0.5, 1, 1.5, 3 and 5 m/s) and the Quercus coccifera load (4 experiments without wind for load values of 3, 4, 5 and 6 kg/m^2). In the present work we will only report on the experiment without wind where the Quercus coccifera load is equal to 3 kg/m^2 to determine the fire front positions and the flame parameters in each zone.

The signals measured by the heat flux sensor are noisy due to the flame oscillations caused by the turbulent flow surrounding the flame. The oscillation frequency of the flame can be estimated at 1 Hz. This low frequency perturbation must be filtered. A low frequency filter, a Butterworth filter, has been considered. The magnitude of the transfer function for this filter is:

$$\left|H(f)\right|^2=\frac{1}{1+(\frac{f}{f_c})^{2n}} \tag{24}$$

In this relation, n is the order of the filter which will be chosen equal to 2 and f, f_c are respectively the frequency and the cut-off frequency. We have chosen a cut-off frequency $f_c=3f_p$ where $f_p=0.0042$ Hz is the characteristic frequency of the propagation. The different heat fluxes given by the thermal sensor are illustrated in Fig. 7.

The distance between the thermocouple i and the thermocouple $i+1$ ($i=\overline{1,4}$) is 75 cm so that the rate of spread in each zone can be given by:

$$ROS\ [\text{cm/s}]=\frac{75}{\Delta t_{i,i+1}} \tag{25}$$

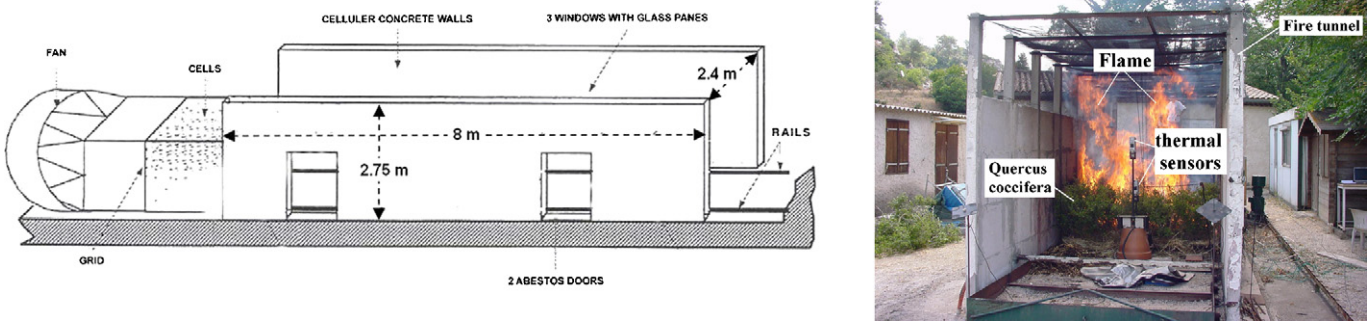

Fig. 5. Diagram and picture of the outside fire tunnel.

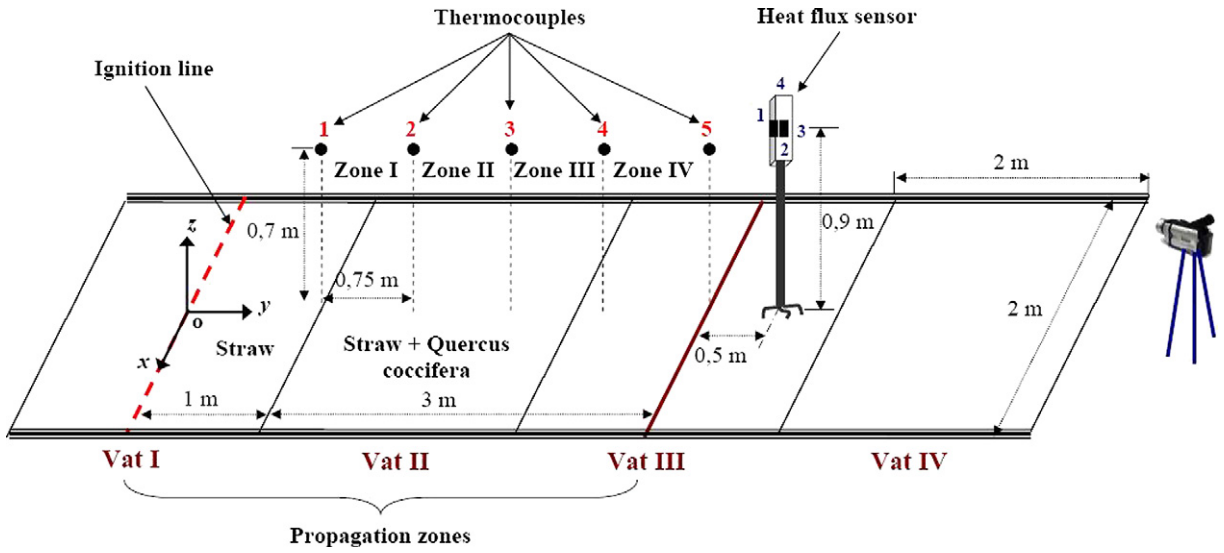

Fig. 6. Diagram showing the positions of the different devices in the fire tunnel.

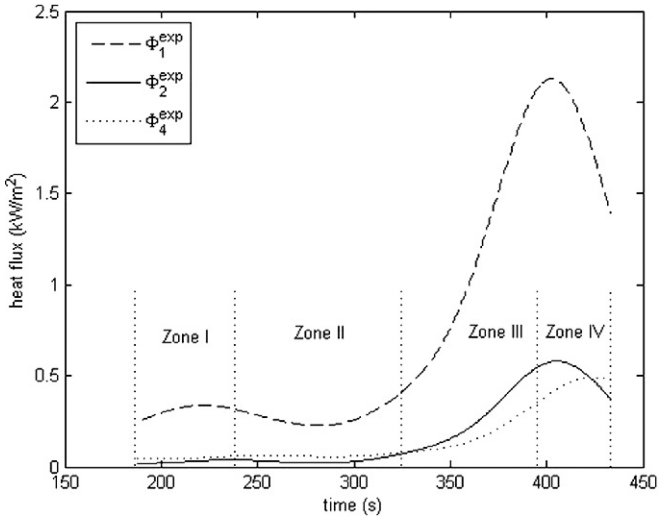

Fig. 7. Heat fluxes given by the thermal sensor in the fire experiment.

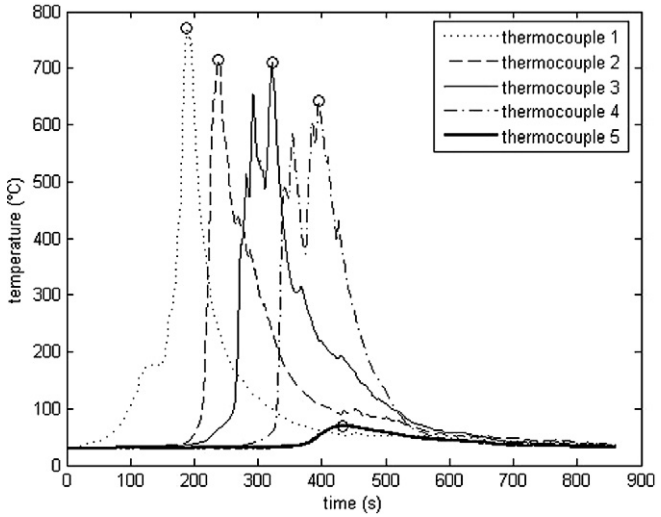

Fig. 8. Different temperatures given by the thermocouples.

Table 2
Experimental values of the rate of spread in the different zones

	Zone I	Zone II	Zone III	Zone IV
Rate of spread [cm/s]	1.50	0.89	1.03	1.97

where $\Delta t_{i,i+1}$ is the time separating two successive temperature peaks. The temperatures measured by the different thermocouples are plotted in Fig. 8 and the rate of spread values are given in Table 2.

5. Identification of the fire positions and flame characteristics

The experimental heat fluxes measured in the fire tunnel experiments described in Section 4 will be used with mathematical modelling to identify the different parameters involved in this one for each propagation zone. These parameters are the flame front positions Y_j, its thickness e_j, the flame height h_f, the temperature T_f and the extinction coefficient K_f of the flame.

5.1. Objective function and optimisation algorithm

In order to identify the fire positions and the flame characteristics the following objective function S will be minimised:

$$S(\eta) = \sum_{j=1}^{N} \left(\Phi_a^{\text{th}}(\eta_j) - \Phi_1^{\text{exp}}(t_j)\right)^2 + \sum_{j=1}^{N} \alpha_j^2 \left(\Phi_l^{\text{th}}(\eta_j) - \Phi_2^{\text{exp}}(t_j)\right)^2 + \sum_{j=1}^{N} \beta_j^2 \left(\Phi_l^{\text{th}}(\eta_j) - \Phi_4^{\text{exp}}(t_j)\right)^2 \quad (26)$$

where $\Phi_k^{\text{exp}}(t_j) = \varphi_k(t_j) - \varphi_3(t_j)$ with $k = 1, 2, 4$ are the experimental heat fluxes measured by the thermal sensor and

Table 3
Values of the flame front positions in the different zones

	Flame front positions Y_j [m]									
Zone I (3.5–2.75 m)	3.49	3.39	3.32	3.21	3.13	3.08	2.99	2.88	2.79	2.71
Zone II (2.75–2 m)	2.74	2.64	2.62	2.47	2.45	2.36	2.27	2.20	2.07	2.00
Zone III (2–1.25 m)	1.92	1.84	1.79	1.72	1.62	1.53	1.46	1.38	1.31	1.21
Zone IV (1.25–0.5 m)	1.21	1.14	1.06	0.97	0.89	0.82	0.74	0.67	0.60	0.54

Table 4
Values of the flame thicknesses in the different zones

	Thicknesses of flame e_j [cm]									
Zone I (3.5–2.75 m)	28	29	30	30	30	30	29	27	25	23
Zone II (2.75–2 m)	23	20	18	15	14	13	13	14	15	17
Zone III (2–1.25 m)	17	19	22	26	30	35	41	46	50	50
Zone IV (1.25–0.5 m)	50	48	45	41	37	33	29	25	21	18

$\eta_j = (Y_j, e_j, h_f, T_f, K_f)$ is the vector of the flame parameters, whose length is equal to 23 if we chose $N = 10$. $\alpha_j = \frac{\Phi_2^{\exp}(t_j)}{\Phi_1^{\exp}(t_j)}$ and $\beta_j = \frac{\Phi_4^{\exp}(t_j)}{\Phi_1^{\exp}(t_j)}$ are the weighting coefficients.

We used a direct search method to solve the optimisation problem given by Eq. (26). This method does not require any information about the gradient of the objective function. As opposed to more traditional optimisation methods that use information about the gradient or higher derivatives to search for an optimal point, a direct search algorithm searches a set of points around the current point, looking for one where the value of the objective function is lower than the value at the current point.

In particular, we employed a special direct search algorithm called the *pattern search* algorithm, cf. [11,12]. This algorithm computes a sequence of points that get closer and closer to the optimal point. At each step, the algorithm searches a set of points, called a mesh, around the current point—the point computed at the previous step of the algorithm. The algorithm forms the mesh by adding the current point to a scalar multiple of a fixed set of vectors called a pattern. If the algorithm finds a point in the mesh that improves the objective function at the current point, the new point becomes the current point at the next step of the algorithm.

5.2. Results and discussion

After the convergence of the algorithm described above, we obtain the different results presented in Tables 3–5. If we use the parameters of these tables to calculate the theoretical heat fluxes given by Eqs. (22) and (23), we can plot their curves with the experimental heat fluxes in Fig. 9.

The rates of spread *ROS* in the four propagation zones are deduced using a linear regression based on the values of the fire front positions. Fig. 10 shows these linear regressions. The different values of the rate of spread are presented in Table 6 with their relative uncertainties.

Let us analyse now the different results. The fire front position values in the four propagation zones are coherent values and the estimated flame thicknesses are close to the observed

Table 5
Values of height, of temperature and of extinction coefficient of the flame in the different zones

		Zone I	Zone II	Zone III	Zone IV
Flame height h_f	Experimental value [m]			1.60	
	Estimated value [m]	1.6	1.59	1.50	1.49
	Relative uncertainty [%]	0	0.63	6.25	6.9
Flame temperature T_f	Experimental value [°C]			751	
	Estimated value [°C]	747	752	751	751
	Relative uncertainty [%]	0.53	0.13	0	0
Flame extinction coefficient K_f[m^{-1}]	Value of Margerit and Séro-Guillaume [6]			0.2	
	Estimated value	0.2	0.2	0.2	0.2

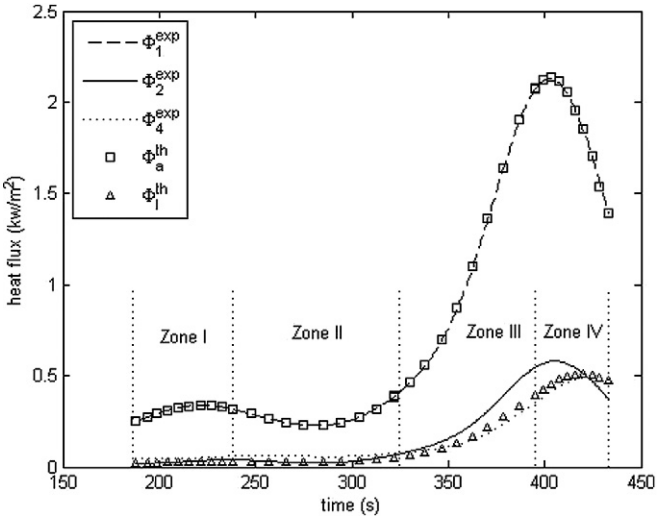

Fig. 9. Theoretical and experimental heat fluxes versus time.

values. The relative uncertainties between the flame heights estimated experimentally by camera and the ones obtained by the theoretical model do not exceed 7%. This value is lower than the appreciation error for traditional yellow flames, 10 to 20%, indicated by Williams, cf. [13]. Let us notice moreover that the identified flame temperatures are very close to the experimental value measured by a thermocouple placed in the flame at a height of 70 cm above the vegetation surface. The extinction

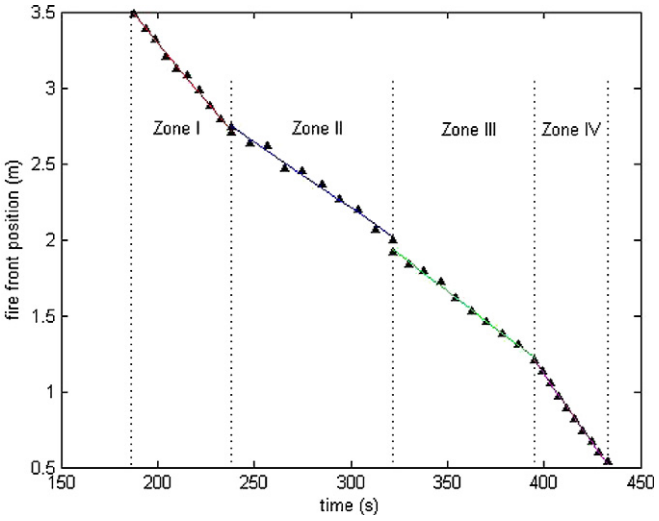

Fig. 10. Fire front positions versus time in the four propagation zones.

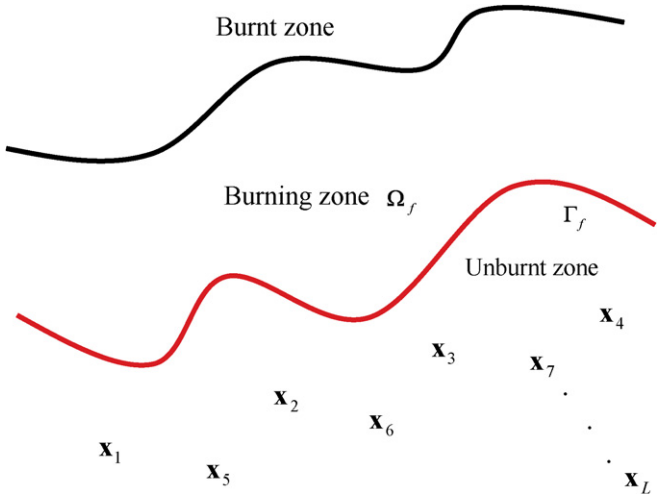

Fig. 11. The fire front and the positions of the heat flux sensors in a real terrain experiment.

Table 6
Estimated values of the rate of spread in the different zones

	Zone I	Zone II	Zone III	Zone IV
Rate of spread [cm/s]	1.54	0.87	0.97	1.80
Relative uncertainty (%)	2.4	1.9	5.5	8.5

coefficients of the flame obtained by inverse method in the different propagation zones are equal to the one given by Margerit and Séro-Guillaume, cf. [6]. The relative gap between the rate of spread given by the linear regression and the one measured by the thermocouples is inferior to 3% in the first and second propagation zones. This value has been exceeded in the third and fourth zones. We can explain this by the uncertainty of the measurements taken by the thermocouples in these zones. The rates of spread have been evaluated assuming that the position of the fire front is given by the successive peaks of temperature. However, one can notice on Fig. 8 that determining the temperature peaks is not easy from the signals given by thermocouples 3 and 4.

The preceding results have been obtained in a fire tunnel where the fire front is a straight line. In a real terrain experiment the fire front will be of any shape, cf. Fig. 11. The preceding algorithm can be extended to this more complex case. In such a terrain, we place L heat flux sensors in $\{\mathbf{x}_1, \ldots, \mathbf{x}_l, \ldots, \mathbf{x}_L\}$ points so that the objective function can be written:

$$S(\eta) = \sum_{l=1}^{L} \Bigg[\sum_{j=1}^{N} \big(\Phi_1^{\text{th}}(\eta_j, \mathbf{x}_l) - \Phi_1^{\text{exp}}(t_j, \mathbf{x}_l)\big)^2 + \sum_{j=1}^{N} \alpha_j^2 \big(\Phi_2^{\text{th}}(\eta_j, \mathbf{x}_l) - \Phi_2^{\text{exp}}(t_j, \mathbf{x}_l)\big)^2 + \sum_{j=1}^{N} \beta_j^2 \big(\Phi_4^{\text{th}}(\eta_j, \mathbf{x}_l) - \Phi_4^{\text{exp}}(t_j, \mathbf{x}_l)\big)^2 \Bigg] \tag{27}$$

where η is the parameters vector containing the different fire front positions and N is its length. $\Phi_k^{\text{exp}}(t, \mathbf{x}_l)$ and $\Phi_k^{\text{th}}(\eta, \mathbf{x}_l)$ with $k = 1, 2, 4$ are respectively the experimental and the theoretical heat fluxes given by the thermal sensor placed on $\mathbf{x}_l$. These theoretical heat fluxes are given by the following expression:

$$\Phi_k^{\text{th}}(\eta, \mathbf{x}_l) = K_f \frac{B}{\pi} \int_{\Omega_f} T_f^4 \frac{(\mathbf{x} - \mathbf{x}_l) \cdot \mathbf{n_k}}{\|\mathbf{x} - \mathbf{x}_l\|^3} \, \mathrm{d}\Omega \tag{28}$$

with Ω_f being the burning zone.

Using an adequate optimisation algorithm, the minimisation of the objective function S given by (27) can provide the fire front positions and the flame parameters for a real fire. A theoretical analysis of the problem has been provided in [14]. In this study a front is considered and some fluxes are calculated on a regular grid containing fire using (28) then the interface or the fluxes values are perturbed to simulate measurement errors. It has been demonstrated that within the context of a flame model, i.e. using (28), the position of the interface can be recovered setting the question as a geometric control problem. In the future, we will validate this technique on one complex experimental scenario, such as prescribed burnings.

6. Conclusion

Some attempts have been made at reconstructing a fire front by image processing video recorded fire, cf. [15,16]. This task is hard because due to smoke the video is really noisy. The work presented here is a first attempt to propose an alternative to image processing in vegetation fire metrology. From the measurement of the heat flux received by a thermal sensor in four directions of space we were able to determine some characteristics of the flame, the positions and the rate of spread of a line fire front.

The aim of this paper is not to discuss the validity of the flame model in propagation models so we have considered a model of isothermal flame. This model, using the inverse method, provides realistic parameters for fire front positions,

flame height, thicknesses of the burning zone, extinction or absorption coefficient ($\sigma_s = 0$) and temperature of flames. However, the present model of flame seems to be a good candidate to modelling the radiative transfer in the propagation models. Let us notice that, as the radiative heat flux is one of the leading processes involved in propagation, it is important for propagation models relying on energy balance [5–8] to have the best flame model possible. The system presented here could help validate a flame model.

Acknowledgements

This research has been done under the support of a national project ANR—P.I.F. (Protection contre les Incendies de Forêts). The authors would like to acknowledge especially Claude Picard and Doctor Frédérique Giroud, from the CEREN, who made valuable recommendations on fire experiments.

Appendix A. Calculation of the transfer function of the thermal sensor

The thermal behaviour of the four heat flux sensors can be represented by a resistor–capacitor model, cf. Fig. A.1.

In the Laplace domain we can write:

$$\begin{pmatrix} \bar{\theta}_{\mathrm{co}_i} \\ \bar{\theta}_{\mathrm{st}} \end{pmatrix} = Z * \begin{pmatrix} \overline{\varphi_i^{\mathrm{exp}}} \\ \overline{\varphi_{\mathrm{st}}} \end{pmatrix} \tag{A.1}$$

and

$$Z = \begin{pmatrix} Z_{11} & Z_{12} \\ Z_{21} & Z_{22} \end{pmatrix} \tag{A.2}$$

where $\bar{\theta}_{\mathrm{co}_i}$, $\bar{\theta}_{\mathrm{st}}$, $\overline{\varphi_i^{\mathrm{exp}}}$ and $\overline{\varphi_{\mathrm{st}}}$ are respectively the Laplace transforms of θ_{co_i}, θ_{st}, φ_i^{exp} and φ_{st}. The different coefficients of the matrix Z are given by:

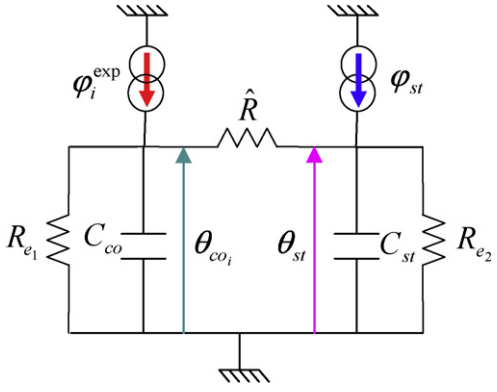

Fig. A.1. Resistor–capacitor model of the thermal sensor.

$$\begin{cases} Z_{11} = \dfrac{Z_{e_1}(\hat{R} + Z_{e_2})}{Z_{e_1} + \hat{R} + Z_{e_2}}, \quad Z_{22} = \dfrac{Z_{e_2}(\hat{R} + Z_{e_1})}{Z_{e_1} + \hat{R} + Z_{e_2}} \\ Z_{12} = Z_{21} = \dfrac{Z_{e_1} Z_{e_2}}{Z_{e_1} + \hat{R} + Z_{e_2}} \end{cases} \tag{A.3}$$

with $Z_{e_1} = \frac{R_{e_1}}{1+R_{e_1} C_{\mathrm{co}} p}$, $Z_{e_2} = \frac{R_{e_2}}{1+R_{e_2} C_{\mathrm{st}} p}$ and p is the Laplace variable.

Using Eqs. (A.1)–(A.3) we can calculate in the time domain the transfer function of the thermal sensor, it is written:

$$\varphi_i^{\mathrm{exp}}(t) = C_{\mathrm{co}} \frac{\mathrm{d}\theta_{\mathrm{co}_i}}{\mathrm{d}t} + \left(\frac{1}{\hat{R}} + \frac{1}{R_{e_1}} \right) \theta_{\mathrm{co}_i} - \frac{1}{\hat{R}} \theta_{\mathrm{st}} \tag{A.4}$$

References

[1] R.-O. Weber, Analytical models for fire spread due to radiation, Combust. Flame 78 (1989) 398–408.
[2] J.-F. Sacadura, Radiative heat transfer in fire safety science, J. Quant. Spectrosc. Radiat. Transfer 93 (2005) 5–24.
[3] K. Chetehouna, O. Séro-Guillaume, A. Degiovanni, C. Picard, F. Giroud, Study of a thermal sensor intended for the calibration of propagation models of forest fires, in: Proceedings of Inverse Problems and Experimental Design in Thermal and Mechanical Engineering, in: Eurotherm Seminar, vol. 68, Edizioni ETS, Poitiers, France, 2001, pp. 287–292.
[4] K. Chetehouna, O. Séro-Guillaume, A. Degiovanni, Identification of the upward gas flow velocity and of the geometric characteristics of a flame with a specific thermal sensor, Int. J. Thermal Sci. 44 (10) (2005) 966–972.
[5] R.-O. Weber, Modelling fire spread through fuel beds, Prog. Energy Combust. Sci. 17 (1991) 67–82.
[6] J. Margerit, O. Séro-Guillaume, Modelling forest fires. Part II: reduction to two-dimensional models and simulation of propagation, Int. J. Heat Mass Transfer 45 (8) (2002) 1723–1737.
[7] A. Simeoni, P.-A. Santoni, M. Larini, J.-H. Balbi, Reduction of a multiphase formulation to include a simplified flow in a semi-physical model of fire spread across a fuel bed, Int. J. Thermal Sci. 42 (1) (2003) 95–105.
[8] X. Zhou, S. Mahalingam, D. Weise, Modeling of marginal burning state of fire spread in live chaparral shrub fuel bed, Combust. Flame 143 (2005) 183–198.
[9] R. Siegel, J. Howell, Thermal Radiation Heat Transfer, fourth ed., Taylor & Francis, New York, 2002.
[10] F.-A. Albini, Wildland fire spread by radiation: A model including fuel cooling by convection, Combust. Sci. Technol. 45 (1985) 101–113.
[11] L.-R. Michael, V. Torczon, Pattern search algorithms for bound constrained minimization, SIAM J. Optim. 9 (4) (1999) 1082–1099.
[12] C. Audet, J.E. Dennis Jr., Analysis of generalized pattern searches, SIAM J. Optim. 13 (3) (2003) 889–903.
[13] F.-A. Williams, Urban and wildland fire phenomenology, Prog. Energy Combust. Sci. 8 (1982) 317–354.
[14] D. Bernardin, O. Séro-Guillaume, On the estimation of the forest fire front position by radiative flux measurement, report of Project ANR "P.I.F.", Inverse Problems, submitted for publication.
[15] E. Pastor, A. Àgueda, J. Andrade-Cetto, M. Muñoz, Y. Pérez, E. Planas, Computing the rate of spread of linear flame fronts by thermal image processing, Fire Safety J. 41 (2006) 569–579.
[16] J.M.-C. Mendes-Lopes, J.M.-P. Ventura, Flame characteristics in fires propagating in beds of Pinus halepensis needles, in: D.X. Viegas (Ed.), V International Conference on Forest Fire Research, CD-ROM, 2006.